

Proton-Gated Rectification Regimes in Nanofluidic Diodes Switched by Chemical Effectors

Gonzalo Pérez-Mitta,* Waldemar A. Marmisolle, Loïc Burr, María Eugenia Toimil-Molares, Christina Trautmann, and Omar Azzaroni*

During the last decade, nanofluidic devices based on solid-state nanopores and nanochannels have come into scene in materials science and will not leave anytime soon. One of the main reasons for this is the excellent control over ionic transport exerted by such devices that promises further important advances when integrated into more complex molecular devices. As a result, pH, temperature, and voltage-regulated devices have been obtained. However, nowadays, there is still a necessity for molecule-driven nanofluidic devices. Here, a sugar-regulated pH-responsive nanofluidic diode is presented obtained by surface modification of conical polycarbonate nanochannels with electropolymerized 3-aminophenylboronic acid. Control over the ionic transport has been achieved by a successful decoration of asymmetric nanochannels with integrated molecular systems. The as-synthesized boronate-appended zwitterionic polymer exhibits an acid-base equilibrium that depends on the concentration of sugar, which ultimately acts as a chemical effector setting different pH-dependent rectification regimes. As a result, the same nanodevice can perform completely different proton-regulated nanofluidic operations, i.e., anion-driven rectification, cation-driven rectification, and no rectification, by simply varying the concentration of fructose in the electrolyte solution.

1. Introduction

Currently, there is a high interest in developing nanofluidic devices that allow regulating the transport of ionic species with experimentally controllable stimuli, such as pH, temperature, light, or the presence of certain molecules in solution.^[1–5] In order to achieve this goal, combining nanofluidic fabrication techniques with different surface modifications, ranging

from organic chemistry to physical methods such as atomic layer deposition or metallic sputtering, is needed.^[6–8] The implementation of the various surface modification techniques allows including different functional groups within nanofluidic structures that confer them the aimed responsive behavior. Among the large variety of nanochannel-fabrication techniques available in literature, ion-track etching technology is the most largely used for a number of reasons. The main reason is that the combination of ion irradiation and chemical etching enables the fabrication of nanochannels with controlled geometry (e.g., cylindrical, conical, and biconical) and size. This, in turn, confers the channels unique iontronic functions, such as rectifiers, diodes, and field-effect transistors.^[9–12] Ionic diodes, for example, are obtained by using conical geometries. Due to the asymmetry in the charge distribution of these nanochannels, a voltage-dependent electrostatic repulsion for ions with the

same charge of the pores is generated and a concurrent rectification in the transmembrane ionic current across the pores arises.


Furthermore, using conical channels, the diode-like behavior has been used to translate specific stimuli in solution into transmembrane current signals under the principle of changing the magnitude and sign of charges on the surface of the channels. A change in the sign of the surface charge generates a concomitant change in the type of ion excluded from the pores, therefore controlling the transport of cations and anions selectively.^[13,14] Therefore, most of the work performed in the field of nanofluidics to modify nanochannels consists of incorporating molecules that change the magnitude and sign of the surface charge under specific stimuli. Moreover, there is further interest in developing multiple responsive systems that allow performing complex nanofluidic operations with the application of two or more stimulus independently or in a coordinated manner. There are examples of such systems that responds to pH and light or pH and temperature.^[15–17]

In this regard, we have shown in a recent report a voltage- and pH-controlled nanofluidic diode by asymmetric electrosynthesis of the conducting polymer polyaniline (PANI)

Dr. G. Pérez-Mitta, Dr. W. A. Marmisollé, Prof. O. Azzaroni
Instituto de Investigaciones Fisicoquímicas Teóricas y Aplicadas (INIFTA)
Universidad Nacional de La Plata – CONICET – CC 16 Suc. 4 (1900)
La Plata, Argentina
E-mail: gperezmitta@inifta.unlp.edu.ar; azzaroni@inifta.unlp.edu.ar

Dr. L. Burr, Dr. M. E. Toimil-Molares, Prof. C. Trautmann
GSI Helmholtz Centre for Heavy Ion Research GmbH
Darmstadt 64291, Germany

Prof. C. Trautmann
Technische Universität-Darmstadt
Darmstadt 64287, Germany

 The ORCID identification number(s) for the author(s) of this article can be found under <https://doi.org/10.1002/smll.201703144>.

DOI: 10.1002/smll.201703144

on a conical track-etched nanochannel previously modified by Au sputtering.^[18] The presence of PANI allowed us to selectively control the transport of ions by applying different electrochemical potentials to the modified membrane or by changing the pH of the solution.

The next step toward the incorporation of nanofluidic devices in integrated molecular circuits with application in biological sciences demands developing systems that can be controlled by the presence of certain molecules of interest in solution. This is an emerging concept stemming from the biomimesis of cells that regulates their functions by the selective passage of ions and molecules across the cellular membrane.

Herein, we developed a pH-responsive nanochannel whose acidic equilibrium can be modulated by the presence of sugars in solution. The fabrication procedure included the electrochemical synthesis of the polyaniline derivative poly(3-aminophenylboronic acid) (PAPBA) on asymmetrically metalized conical track-etched polycarbonate nanochannels. PAPBA bears a boronate group in each monomer that confers a negative charge that competes with the positive charges from the nitrogen-containing functional groups in the backbone, thus enabling the occurrence of charge inversion around the isoelectric point (IP) of the PAPBA. Furthermore, due to the tendency of the boronates to form complexes with diols modifying the acidic constants of the native form, it is possible to modulate the pH responsiveness with the concentration of sugar in solution, e.g., fructose. We should note that sugar sensing in nanofluidic devices has been investigated in the past;^[19–22] however,

rather than focusing on the sensing capabilities of PAPBA-modified nanopores, the purpose of this work is to explore new avenues to gain “chemical” control over the ionic transport properties of nanofluidic elements by using chemical effectors to set different pH-controlled transport regimes.

2. Results and Discussion

To characterize the geometry of the nanochannels, two different approaches were used. Both direct cross-section SEM imaging and nanochannels-templated Au nanoneedles fabrication were employed (**Figure 1**) and second, a template method was used. For the latter case, gold was electrodeposited potentiostatically in multichannel track-etched membranes synthesized under the same conditions as the single-channel membranes. After the subsequent dissolution of the polycarbonate foil, the resulting cones were imaged by SEM (**Figure 1a,b**). The resulting images showed conical geometries with a tip diameter of ≈ 60 nm and a base of ≈ 4000 nm.^[23] As expected for nanochannels with such large tips, they exhibited symmetric (ohmic) ion transport, without any rectification. It was shown previously that for conical geometries, tip diameters of below 20–30 nm are required for ionic current rectification. Only for geometries of enhanced asymmetry toward the tip (e.g., bullet-like or parabolic geometry), the minimum diameter to observe rectification can be greater than these values.^[24–27]

Once current–voltage (I – V) characteristics of the gold-sputtered-nanochannels were measured, PAPBA was electrosynthesized

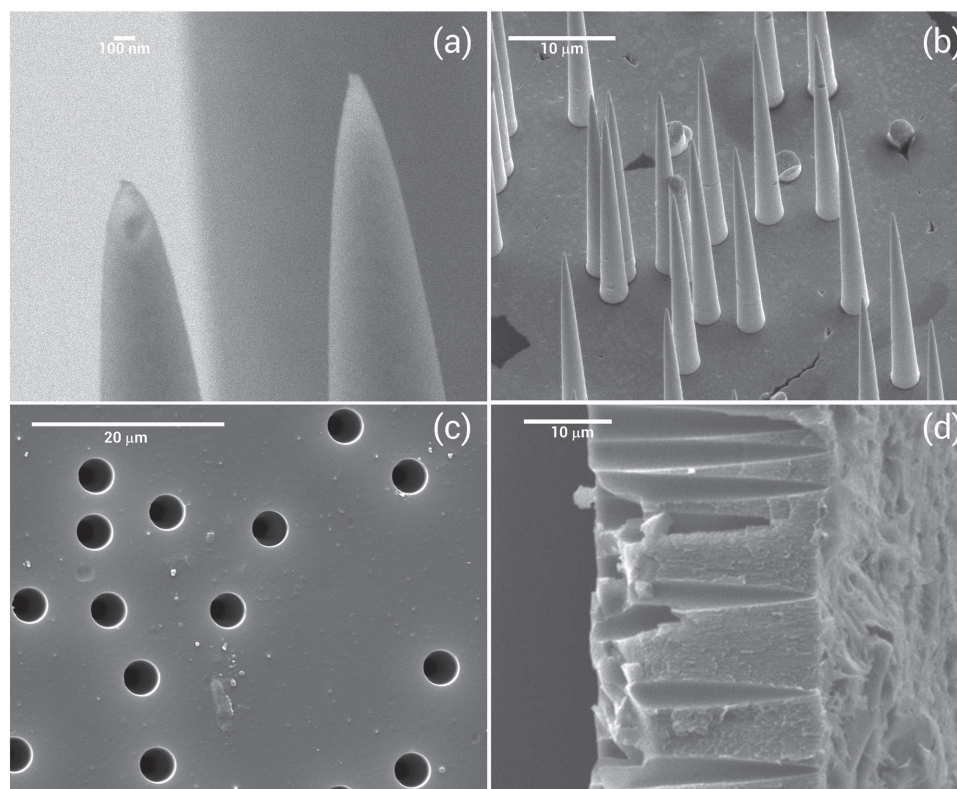


Figure 1. SEM images taken at a) 90° and b) 30° of gold nanocones fabricated by the track-etched template method. Figure (a) shows tip diameters of ≈ 60 nm. c) SEM image of the side of a track-etched polycarbonate displaying the large opening of conical nanochannels in a multitrack foil (10^9 tracks cm^{-2}). d) Cross-section SEM image of a multitrack PC foil containing conically etched nanochannels.

potentiodynamically on the Au-metallized surface of the nanochannels as explained in the Experimental Section (Figure 2a).^[28]

In order to approximate the thickness of the PAPBA layer electrosynthesized on top of the nanochannel-containing foils, surface plasmon resonance (SPR) measurements were performed during the electrochemical synthesis of PAPBA on a planar gold electrode under identical conditions than for the electrochemical growth on the metallized membranes. (Figure 2b). The results revealed a deposition rate of 1.5 nm per cycle. Thus, we estimate that a 45 nm-thick PAPBA layer was deposited on the gold-sputtered nanochannels. SEM imaging of the closing of the nanochannels was performed showing a reduction of ≈ 60 nm of the initial diameter which correlates with a thickness of PAPBA of 30 nm (Figure S1, Supporting Information). Even though there is a difference of a 50 % between the SEM images and SPR determination, it has to be taken into account that the SEM pictures are taken in high vacuum and dry conditions, and therefore the polymer is expected to be collapsed. Furthermore, taking into account that the sputtering process generates a reduction of 10 nm of the tip diameter—leading to a size of 50 nm after the metallization—the expected diameter of the nanochannel after the polymerization is ≈ 5 nm.

The chemical nature of the electrosynthesized polymer was confirmed by Raman spectroscopy (Figure 2c). The more

intense Raman bands appear in the range $1000\text{--}1700\text{ cm}^{-1}$ and the spectrum is dominated by the well-established bands of the PANI-based polymers.^[29,30] The C-H in-plane bending modes appear at about 1160 cm^{-1} ,^[31] whereas the bands assigned to the CN stretching appear at about $1310\text{--}1400\text{ cm}^{-1}$ (radical cation) and $1470\text{--}1490\text{ cm}^{-1}$ (quinone diimine).^[32] The C=C stretching of the quinoid units is at about $1570\text{--}1595\text{ cm}^{-1}$ and its presence is related to the conducting form of the polymer.^[33,34] The features due to the presence of the boronic moiety are expected to be at about 900 and 1100 cm^{-1} for the stretching of the B-F bond^[35–37] and the bending modes of the B-OH moiety respectively and at about 1330 cm^{-1} for the stretching mode of the B-O bond.^[37–41] The position of these peaks is within the region of intense peaks of the PANI-like structure, so their presence was confirmed by comparison of the Raman spectrum of PAPBA with that of PABA (poly(3-aminobenzylamine)), which is a similar PANI-like polymer without boronic moieties.^[42] Arrows in this figure indicate the position of these bands characteristic of the boronic group. The bands at 900 and 1100 cm^{-1} are clearly noticeable, whereas the band predicted at about 1330 cm^{-1} appears as a shoulder of the intense PANI-like band in this region. After incubation in $100 \times 10^{-3}\text{ M}$ fructose solution for 1 h, this shoulder assigned to the asymmetric stretching of the B-O increases as a consequence of the formation of the cyclic ester

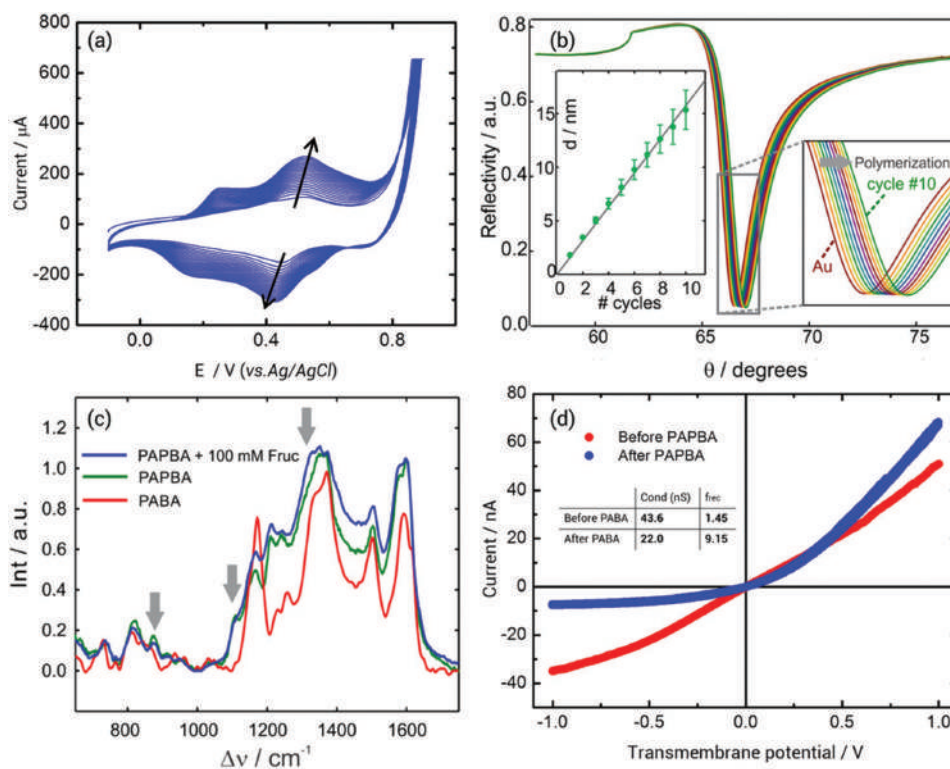


Figure 2. a) Cyclic voltammety of the electropolymerization of PAPBA over a metallized single nanochannel-containing polycarbonate membrane. Arrows indicate increasing cycles b) SPR angular scan curves for different number of voltammety cycles during the electrosynthesis of a PAPBA film on Au. Values of the thickness determined by the fitting of the curves are presented in the inset. A deposition rate of 1.5 nm per cycle was obtained by linear fitting. c) Background-corrected Raman spectra of PAPBA films electrosynthesized on Au. The spectrum of a PABA film was added for comparison. d) I - V curves for a PC nanochannel before and after the polymerization of PAPBA. Inset: Values of ionic conductance and rectification ratios for the nanochannel before and after the modification.

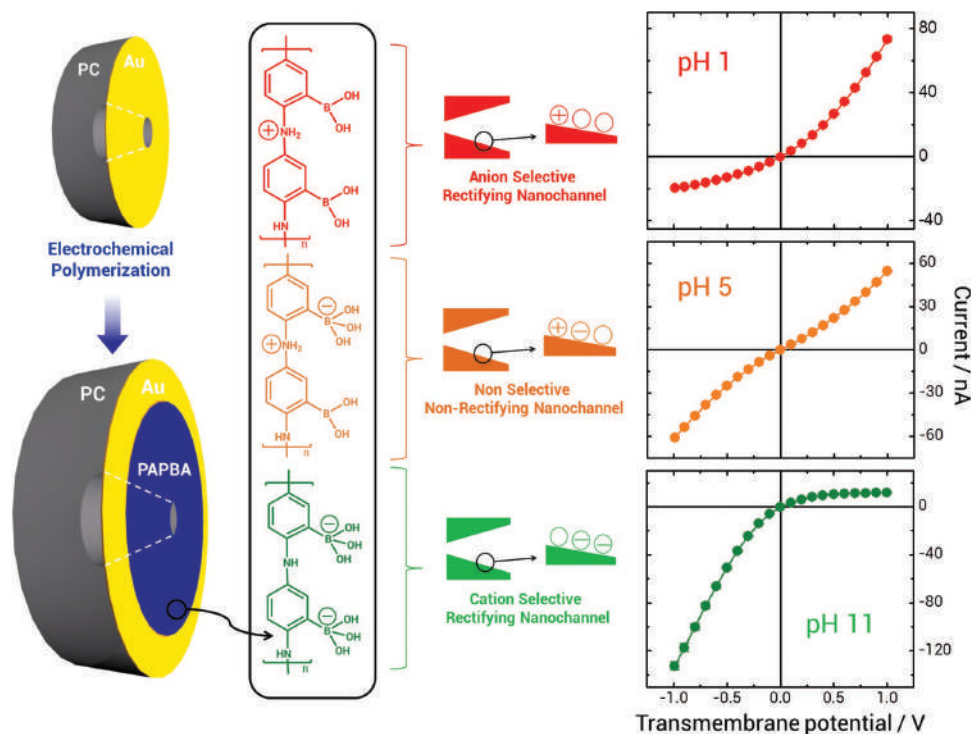


Figure 3. Scheme depicting the functionalization of a metallized polycarbonate nanochannel and the charge state of the channel related to current-voltage measurements for pH 1 (red), 5 (orange), and 11 (green) in 0.1 M KCl solution.

with the sugar.^[37,40,43] Also, the increase of the signal at about 1200 cm^{-1} could be due to the stretching of C-O modes of the sugar, which has been reported at 1225 cm^{-1} .^[37]

I-*V* using a 0.1 M KCl solution, before and after the polymerization of PAPBA showed that there was a reduction of a 50% of the ionic conductance of the nanochannel, from ≈ 44 to 22 nS. Also, a large increment in the rectification efficiency was observed (Figure 2d). The rectification efficiency is characterized by the rectification factor f_{rec} defined in this case as the ratio between the currents at 1 V and the current at -1 V .^[44] After the electropolymerization, a change in the f_{rec} from 1.4 (no rectification) to 9 (high rectification) was observed. Due to the fact that the PAPBA was grown only on one side of the membrane, a strong asymmetry on the longitudinal charge distribution of the nanochannel is expected and therefore an increment of the current rectification in the *I*-*V* characteristics.

PAPBA is a zwitterionic polymer that becomes either positively or negatively charged at pHs lower or higher than its IP, respectively (scheme in Figure 3).^[45] Positive charges stem from the secondary amines present in the backbone of the polymer, while negative charges arise from the boronate pendant groups. The presence of these acid-base groups results in a pH dependence of the surface charge of PAPBA-modified nanochannels.^[46] As the limitation in the accuracy of the regulation of the ionic current rectification is related to the capacity of modulating the surface charge, protonable macromolecules such as PAPBA, which presents a continuous acid-base equilibrium, allow obtaining a fine tuning of the rectification features by changing the pH.

Figure 3 shows current-voltage curves obtained for a PAPBA-modified single nanochannel at three different pH values. Positive (anion-driven), neutral (nonselective), and negative

(cation-driven) rectification can be observed for pH 1, 5, and 11, respectively. Positive rectification stems from the presence of positive charges in the nitrogen groups (secondary amines or imine) of the PAPBA polymer. Increasing the pH starts deprotonating PAPBA amines and allows the formation of complex of boronate groups with hydroxyl ions. The first effect is the neutralization of amines positive charges leaving to a nonrectifying state. Further increments of the pH produce a reversion of the charge to negative values with a consequent reappearance of the rectification, but in the opposite direction. The fact that we could observe a reversion of rectification poses an advantage with respect of our previous work using PANI as functional molecule. In that case, it was not possible to achieve a reversion of the surface charge due to the fact that polyaniline does not have negative functional groups.^[18]

Current-voltage curves were measured in 0.1 M KCl with dropwise additions of HCl and NaOH to adjust the pH at different values. In order to study the pH-related changes in the rectification, f_{rec} were calculated as a ratio between the currents at 1 and -1 V where the current placed in the numerator was the higher one, e.g., the current at -1 V for the curve at pH 11, but the current at 1 V for pH 1. Furthermore, in order to correspond a particular rectification factor to a certain state of charge of the PAPBA film, the f_{rec} values when the higher current was at transmembrane voltages $>0\text{ V}$ were multiplied by -1 . This ultimately allows correlating positive f_{rec} with protonated PAPBA and negative f_{rec} with OH^- coordinated PAPBA (Figure 4). By measuring *I*-*V* curves at different pH, apparent titration curves for a PAPBA-modified nanochannel could be obtained. We named these experiments “nanofluidic titration” due to its fundamental resemblance with Zeta-potential titration,

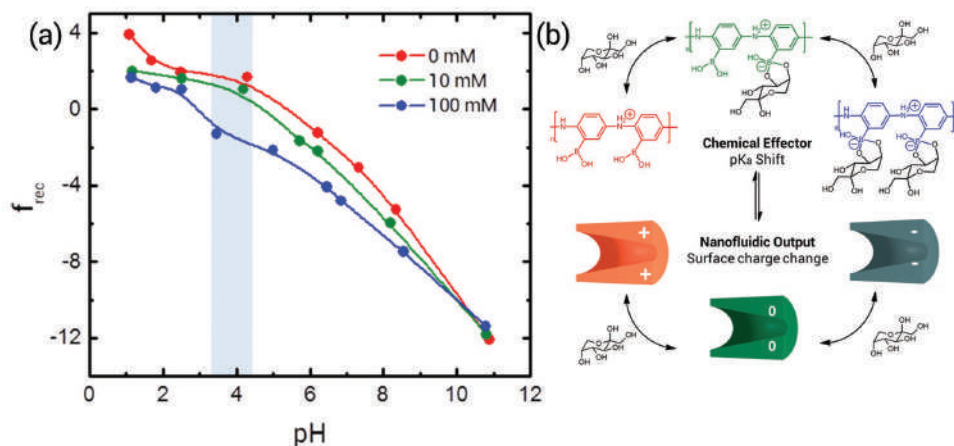


Figure 4. a) Rectification factor versus pH for different concentrations of fructose, namely, 0×10^{-3} M (red), 10×10^{-3} M (green), and 100×10^{-3} M (blue). The blue shadow lies at the inversion region, the region where the fructose produces a reversion of the rectification at a fixed pH. b) Scheme depicting both the chemical change and the surface charge change for different concentrations of fructose.

i.e., f_{REC} evolves in a similar fashion to the change of the surface charge of the nanochannel.^[47,48] This nanofluidic method could be generalized and used for a large number of molecules, such as proteins, polyelectrolytes, or surfactants, among others.^[49,50]

The ability of boronic acids to bind 1,2 or 1,3 diols to form five- or six-membered cyclic esters is well documented.^[51] Binding of boronates with cis-diols like the ones present in monosaccharides is known to be stronger than for acyclic diols or trans-diols. The complex between boronates and sugars has a different pK_a than the boronate itself; therefore the binding of monosaccharides can be sensed as a change in the protonation degree caused by a pK_a shift. In this regard, there are many examples of potentiometric sensors of sugars that make use of this property of boronates present in PAPBA.^[52,53] However, even though this change of the acid-base behavior of PAPBA upon binding of sugars is generally acknowledged, to our knowledge, the modification of the charge state of the polymer has not been experimentally determined in previous studies.

To address this issue, nanofluidic titration curves using different concentrations of a sugar for a pH range from 1 to 11 were obtained. Up to our knowledge, this is the first time that the changes of the charge state of PAPBA, always assumed to occur as a consequence of a putative pK_a shift, are directly monitored. Fructose was used as case of study because it has been proved to have a stronger binding to boronate than other saccharides.^[52] Titration curves were made by measuring current–voltage characteristics in absence of fructose as well as with two different concentrations: 10 and 100×10^{-3} M (Figure 4).

Titration curves show the potentiality of using sugars as chemical effectors to perform complex nanofluidic operations like cation–anion selectivity switching and ion gating. By using fructose as a representative saccharide, shifts in the local acid–base equilibrium within the nanochannel can be produced triggering different nanofluidic regimes, as we explain below.

As it can be observed in Figure 4, fructose acts as an effector for almost the complete range of pH. However, the most interesting control exerted by fructose over nanofluidic operations laid within the range between pH 1 and 8. Four different regions of the effect that sugars produces at different pH were observed.

The effect of sugar concentration on the rectification behavior is presented in the Supporting Information for the case of pH 7. The value of the rectification factor increases as a function of the sugar concentration finally reaching an asymptotic plateau which reflects a simple binding response.^[20,21] Values of f_{REC} practically do not change from 60 to 100×10^{-3} M of fructose, which indicates that the binding sites are nearly saturated. Therefore, current–voltage curves at 0 and 100×10^{-3} M fructose were measured within the different pH ranges to inspect the effect of the sugar-free and sugar-bound states respectively on the nanofluidic behavior of the nanochannel.

The first region, which will be referred as acid region for being located at $pH \approx 1$ –2, is characterized by a transition between a positively charged state (anion-selective) to a non-charged state (nonselective) of the nanochannel surface as shown in Figure 5a. In this region, the effect of adding sugar to the solution is a shutting of the current at positive voltages that corresponds to anions flowing from the tip to the base and cations from the base to the tip. This produces a decrease in the rectification efficiency (loss of selectivity) from a diode-like into an ohmic behavior (Figure 5e).

The second region, also located in a narrow window of pH, is between ≈ 3 and ≈ 4.5 . Using a more functional criterion, this region will be referred as inversion region and it was marked as a shadow in Figure 4. It is called like this because, within this range of pH, the presence of sugar in solution produces an inversion of the surface charge of the nanochannel, thus changing the system from anion-selective to cation-selective. The nanofluidic output of this effect is a change in the direction of the current rectification of the nanochannel as seen in Figure 5b,e.

The third region, named neutral region, located at $pH 6$ –7, presents the opposite operation of the acid region. In this case, the presence of sugars in solution triggers the appearance of negative surface charges, thus enhancing the ionic current rectification by selectively decreasing the ionic current at positive potentials (Figure 5c,e). Then, the nanochannel becomes cation-selective.

The last region for sugar-effected operations, named alkaline region, is located at pH between 7 and 11. Within

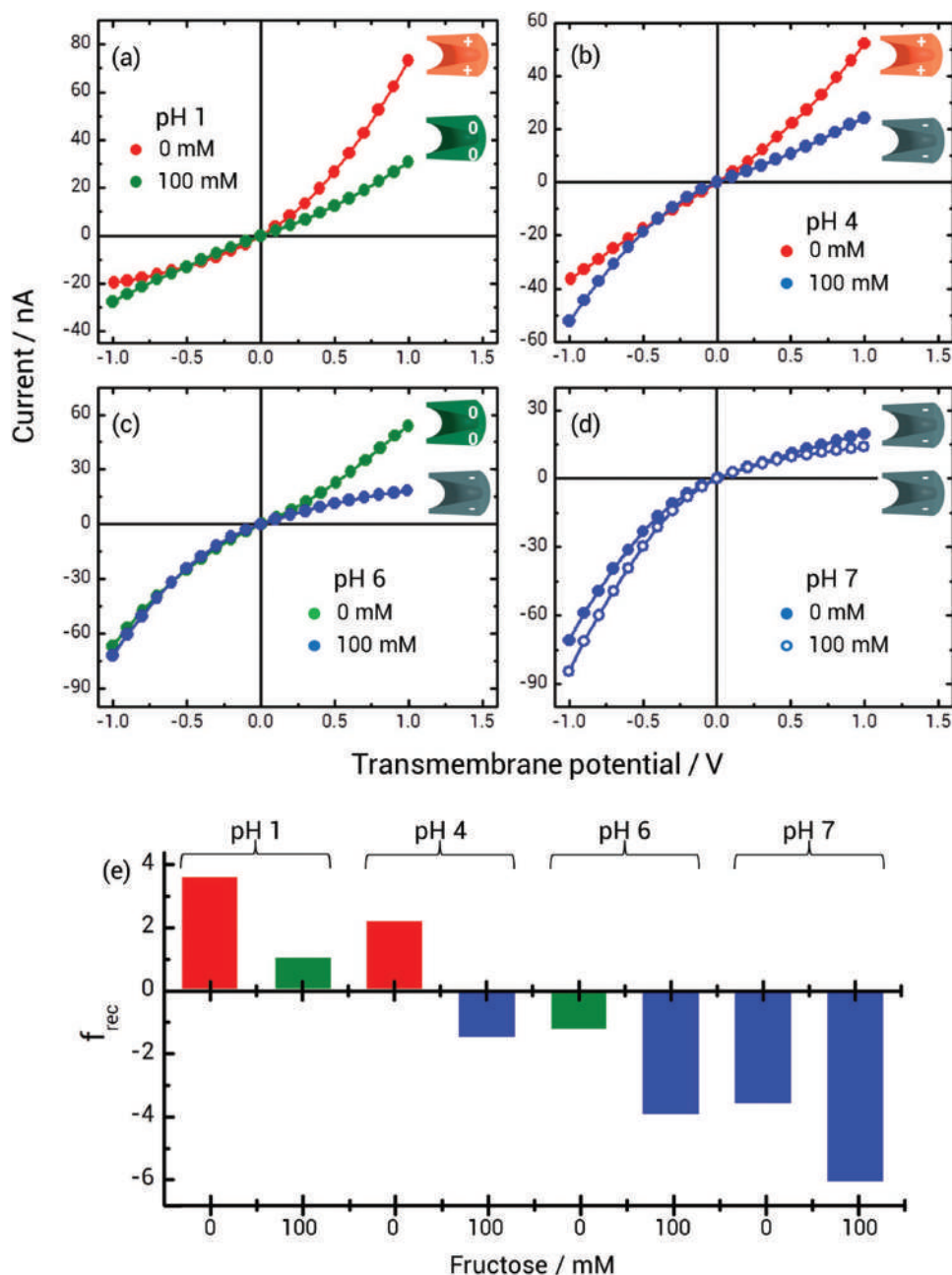


Figure 5. Current–voltage curves for a PAPBA modified nanochannel measured for each of the four regions within the pH-effector range (1–8) in absence and presence of fructose: a) acid, b) inversion, c) neutral, and d) alkaline regions. e) Rectification factors (f_{rec}) calculated for each region in absence and presence of fructose.

this region, the presence of sugar shifts the equilibrium toward the formation of boronate-sugar complex making the negatively charged channel surface even more negative. The nanofluidic output of this effect is the increase in both ionic currents at negative potentials and rectification factors (Figure 5d,e).

The effect of sugars in the alkaline region decreases for higher pH, becoming negligible at pH higher than 9. This feature was expected, since high values of pH are far above the pK_a of the boronate of the polymer, both in the sugar-free and sugar-bound states. Therefore, the degree of negative charge

(and rectification) is at its maximum value irrespectively of the sugar concentration.

The aforementioned results show that there is a wide range of nanofluidic operations that can be performed by using combinations of pH and sugar concentrations in solution within a pH range of 1–8. The switching of the acid-base equilibrium by formation of boronate-sugar complexes allows performing on–off gating of rectification in the acid and neutral regions, while it allows reversing the direction of the current rectification in the inversion region or increasing the cation-driven current in the alkaline region (Figure 5e).

Due to the fact that PAPBA-modified nanochannels are ultimately responsive to fructose, it becomes natural to think in this system as a potential sugar sensor. However, for developing a biosensor based on these procedures, higher efforts need to be done in order to improve the sensitivity of the device and enhance the detection limits.

3. Conclusions

Herein, we have presented the construction of a sugar-regulated pH-responsive nanofluidic diode by integrating an electropolymerized responsive layer of PAPBA to a previously metallized track-etched polycarbonate single nanochannel. The change in the pH-dependent diode-like behavior (rectification factors) with the concentration of fructose reveals the alteration of the net surface charge caused by the shift of the pK_a of the boronic moieties induced by the sugar binding. It was shown that the presence of sugar produces a strong effect in the nanofluidic output of the device by triggering different responses within a wide pH range from 1 to 8. Four regions of actuation were found: acid (gating of anion-driven current), inversion (selectivity reversion), neutral (gating of cation-driven current), and alkaline (enhancement of cation-driven current).

4. Experimental Section

Materials: Synthetic nanopores were fabricated in polycarbonate foils (PC) (Makrofol N, Bayer Leverkusen) of thickness 30 μm . 3-aminophenylboronic acid and KF were purchased from Sigma-Aldrich and used as received.

Etching Procedure: PC foils were irradiated with Au ions (25+) at the UNILAC (Universal Linear Accelerator) of GSI, Darmstadt at an energy of 11.2 MeV per nucleon. Both single- and multiple-ion irradiated PC foils were etched conically using a mixture of methanol:6 M NaOH as etchant (60:40) while applying an electrostopping potential of -1 V throughout the process. The etching was held for 30 min after the breakthrough. The resulting nanochannels had a base diameter (D) ≈ 4000 nm and a tip diameter of (d) ≈ 60 nm as it was reported by the analysis of scanning electron microscopy images (Figure 1).

Electrochemical Synthesis of Poly(3-Aminophenylboronic Acid): First, a layer of 80 nm of gold was sputtered over the tip side of the foils (in the direction normal to the surface). Typically, the nanochannels still did not present rectification or it was very low ($f_{\text{rec}} < 2$) after the metallization. Previous results have shown that the nanochannels report a reduction of the diameter of ≈ 10 nm due to the sputtering. Once the metallized foils were characterized by I - V measurements, they were placed in a two-compartment electrochemical cell (Figure S4, Supporting Information). An external copper ring was used as electric contact between the metallized foil and the potentiostat (Gamry Reference 600). The reference electrode was Ag/AgCl/3 M NaCl. All potentials informed in this work are relative to this electrode. The electrosynthesis solution was 0.05 M 3-amino-phenylboronic acid solution in 0.2 M KF and 0.5 M HCl. The PAPBA was deposited potentiodynamically performing a total of 30 cycles between -0.1 and 0.9 V at 0.1 V s^{-1} (Figure 2a).

Conductivity Measurements: Current-voltage characteristics were obtained using a potentiostat (Gamry Reference 600) with a four-electrode setup (working, working sense, reference-, and counterelectrode) in order to measure single-pore nanochannel conductance variations arising from changes in the nanochannel and not from processes at the surface of the electrodes. Both the working- and counterelectrode were made of platinum, while the reference and working-sense were commercial Ag/AgCl/3 M NaCl electrodes. Measurements were performed in a

homemade conductivity cell fabricated to avoid current leakage. For all the experiments, the working electrode was placed at the base side of the nanochannel, while the counterelectrode was placed at the tip side. The voltage was swept between -1 and 1 V at a speed of 1 V s^{-1} . 0.1 M KCl solution was used as electrolyte. The same experimental setup has been used for all the experiments to unambiguously correlate I - V curves with nanopore surface charges. For such correlation, a rectification factor (f_{rec}) was defined to quantify the rectification efficiency as

$$f_{\text{rec}} = \pm \left| \frac{I(1\text{V or } -1\text{V})}{I(-1\text{V or } 1\text{V})} \right| \quad (1)$$

Here, the current in the numerator is the largest current value corresponding to the higher conductance state, while the one in the denominator is the lowest current value corresponding to the lower conductance state. Additionally, if the higher current corresponds to a negative voltage, then the rectification factor is multiplied with -1 . This definition allows assigning a negative f_{rec} to negative surface charges and positive f_{rec} to positive surface charges. This definition simplifies the interpretation of the experimental results in terms of surface charge.

Information about the SPR and Raman measurements as well as the fabrication of metal nanocones and cross-section imaging can be found in the Supporting Information.

Supporting Information

Supporting Information is available from the Wiley Online Library or from the author.

Acknowledgements

Authors acknowledge financial support from ANPCyT (PICT 2010-2554, PICT-2013-0905, and PPL 2011-003) and from the Deutsche Forschungsgemeinschaft (DFG-FOR 1583). G.P.-M. acknowledges CONICET for a doctoral fellowship. O.A. and W.A.M. are staff members of CONICET. M.E.T.-M. and C.T. acknowledge support by the LOEWE project iNAPO funded by the Hessian State Ministry of Higher Education, Research and Arts.

Conflict of Interest

The authors declare no conflict of interest.

Keywords

chemical actuation, ionic diodes, ionic rectification, nanofluidic devices, solid-state nanopores

Received: September 11, 2017

Revised: December 7, 2017

Published online: February 5, 2018

- [1] Y. Shang, Y. Zhang, P. Li, J. Lai, X.-Y. Kong, W. Liu, K. Xiao, G. Xie, Y. Tian, L. Wen, L. Jiang, *Chem. Commun.* **2015**, 51, 5979.
- [2] W. Guo, H. Xia, F. Xia, X. Hou, L. Cao, L. Wang, J. Xue, G. Zhang, Y. Song, D. Zhu, Y. Wang, L. Jiang, *ChemPhysChem* **2010**, 11, 859.
- [3] G. Pérez-Mitta, A. G. Albesa, W. Knoll, C. Trautmann, M. E. Toimil-Molares, O. Azzaroni, *Nanoscale* **2015**, 7, 15594.
- [4] L. Wen, X. Hou, Y. Tian, F. Q. Nie, Y. Song, J. Zhai, L. Jiang, *Adv. Mater.* **2010**, 22, 1021.

- [5] G. Pérez-Mitta, A. G. Albesa, C. Trautmann, M. E. Toimil-Molares, O. Azzaroni, *Chem. Sci.* **2017**, *8*, 890.
- [6] L. Wen, Y. Tian, J. Ma, J. Zhai, L. Jiang, *Phys. Chem. Chem. Phys.* **2012**, *14*, 4027.
- [7] X. Hou, H. Zhang, L. Jiang, *Angew. Chem., Int. Ed.* **2012**, *51*, 5296.
- [8] A. Spende, N. Sobel, M. Lukas, R. Zierold, J. C. Riedl, L. Gura, I. Schubert, J. M. M. Moreno, K. Nielsch, B. Stühn, C. Hess, C. Trautmann, M. E. Toimil-Molares, *Nanotechnology* **2015**, *26*, 335301.
- [9] I. Vlasiouk, S. Smirnov, Z. Siwy, *ACS Nano* **2008**, *2*, 1589.
- [10] Z. Siwy, P. Apel, D. Dobrev, R. Neumann, R. Spohr, C. Trautmann, K. Voss, *Nucl. Instrum. Methods Phys. Res., Sect. B* **2003**, *208*, 143.
- [11] E. B. Kalman, I. Vlasiouk, Z. S. Siwy, *Adv. Mater.* **2008**, *20*, 293.
- [12] Y. Ai, J. Liu, B. Zhang, S. Qian, *Sens. Actuators, B* **2011**, *157*, 742.
- [13] B. Yameen, M. Ali, R. Neumann, W. Ensinger, W. Knoll, O. Azzaroni, *Nano Lett.* **2009**, *9*, 2788.
- [14] B. Yameen, M. Ali, R. Neumann, W. Ensinger, W. Knoll, O. Azzaroni, *J. Am. Chem. Soc.* **2009**, *131*, 2070.
- [15] Y.-B. Zheng, S. Zhao, S.-H. Cao, S.-L. Cai, X. Cai, Y.-Q. Li, *Nanoscale* **2017**, *9*, 433.
- [16] L. Wen, Q. Liu, J. Ma, Y. Tian, C. Li, Z. Bo, L. Jiang, *Adv. Mater.* **2012**, *24*, 6193.
- [17] H. Zhang, X. Hou, L. Zeng, F. Yang, L. Li, D. Yan, Y. Tian, L. Jiang, *J. Am. Chem. Soc.* **2013**, *135*, 16102.
- [18] G. Pérez-Mitta, W. A. Marmisollé, C. Trautmann, M. E. Toimil-Molares, O. Azzaroni, *J. Am. Chem. Soc.* **2015**, *137*, 15382.
- [19] Q. H. Nguyen, M. Ali, R. Neumann, W. Ensinger, *Sens. Actuators B* **2012**, *162*, 216.
- [20] B. Vilozny, A. L. Wollenberg, P. Actis, D. Hwang, B. Singaram, N. Pourmand, *Nanoscale* **2013**, *5*, 9214.
- [21] S. Zhao, Y.-B. Zheng, S.-L. Cai, Y.-H. Weng, S.-H. Cao, J.-L. Yang, Y.-Q. Li, *Electrochem. Commun.* **2013**, *36*, 71.
- [22] Y.-B. Zheng, S. Zhao, S.-H. Cao, S.-L. Cai, X. Cai, Y.-Q. Li, *Nanoscale* **2017**, *9*, 433.
- [23] L. Burr, *PhD Thesis Germany* **2016**, <https://doi.org/10.13140/RG.2.1.3768.7286>.
- [24] P. Y. Apel, I. V. Blonskaya, O. L. Orelovitch, S. N. Dmitriev, *Nucl. Instrum. Methods Phys. Res., Sect. B* **2009**, *267*, 1023.
- [25] P. Ramírez, P. Y. Apel, J. Cervera, S. Mafé, *Nanotechnology* **2008**, *19*, 315707.
- [26] Z. S. Siwy, *Adv. Funct. Mater.* **2006**, *16*, 735.
- [27] M. L. Kovarik, K. Zhou, S. C. Jacobson, *J. Phys. Chem. B* **2009**, *113*, 15960.
- [28] B. Fabre, L. Taillebois, *Chem. Commun.* **2003**, *1*, 2982.
- [29] W. A. Marmisollé, O. Azzaroni, *Nanoscale* **2016**, *8*, 9890.
- [30] Z. Morávková, M. Trchová, M. Exnerová, J. Stejskal, *Thin Solid Films* **2012**, *520*, 6088.
- [31] M. Bartonek, N. S. Sariciftci, H. Kuzmany, *Synth. Met.* **1990**, *36*, 83.
- [32] Y. Furukawa, F. Ueda, Y. Hyodo, I. Harada, T. Nakajima, T. Kawagoe, *Macromolecules* **1988**, *21*, 1297.
- [33] S. Quillard, K. Berrada, G. Louam, S. Lefrant, *Synth. Met.* **1995**, *69*, 201.
- [34] R. Mazeikiene, A. Statino, Z. Kuodis, G. Niaura, A. Malinauskas, *Electrochem. Commun.* **2006**, *8*, 1082.
- [35] B. A. Deore, M. S. Freund, *Chem. Mater.* **2005**, *17*, 2918.
- [36] Y.-P. Zhang, S.-H. Lee, K. R. Reddy, A. I. Gopalan, K.-P. Lee, *J. Appl. Polym. Sci.* **2007**, *104*, 2743.
- [37] C. L. Recksiedler, B. A. Deore, M. S. Freund, *Langmuir* **2005**, *21*, 3670.
- [38] S. Li, Q. Zhou, W. Chu, W. Zhao, J. Zheng, *Phys. Chem. Chem. Phys.* **2015**, *17*, 17638.
- [39] J. A. Faniran, H. F. Shurvell, *Can. J. Chem.* **1968**, *46*, 2089.
- [40] B. A. Deore, M. S. Freund, *Chem. Mater.* **2005**, *17*, 2918.
- [41] Y.-P. Zhang, S.-H. Lee, K. R. Reddy, A. I. Gopalan, K.-P. Lee, *J. Appl. Polym. Sci.* **2007**, *104*, 2743.
- [42] W. A. Marmisollé, D. Gregurec, S. Moya, O. Azzaroni, *ChemElectroChem* **2015**, *2*, 2011.
- [43] J. A. Faniran, H. F. Shurvell, *Can. J. Chem.* **1968**, *46*, 2089.
- [44] G. Pérez-Mitta, A. Albesa, F. M. Gilles, M. E. Toimil-Molares, C. Trautmann, O. Azzaroni, *J. Phys. Chem. C* **2017**, *121*, 9070.
- [45] B. Yameen, M. Ali, R. Neumann, W. Ensinger, O. Azzaroni, W. Knoll, *Chem. Commun.* **2010**, *46*, 1908.
- [46] G. Pérez-Mitta, A. G. Albesa, M. E. Toimil Molares, C. Trautmann, O. Azzaroni, *ChemPhysChem* **2016**, *17*, 2718.
- [47] V. Ball, *Colloids Surf., A* **2010**, *363*, 92.
- [48] V. Ball, J. Gracio, M. Vila, M. K. Singh, M.-H. Metz-Boutigue, M. Michel, J. Bour, V. Toniazzo, D. Ruch, M. J. Buehler, *Langmuir* **2013**, *29*, 12754.
- [49] G. Pérez-Mitta, J. S. Tuninetti, W. Knoll, C. Trautmann, M. E. Toimil-Molares, O. Azzaroni, *J. Am. Chem. Soc.* **2015**, *137*, 6011.
- [50] M. Ali, B. Yameen, R. Neumann, W. Ensinger, W. Knoll, O. Azzaroni, *J. Am. Chem. Soc.* **2008**, *130*, 16351.
- [51] H. S. Mader, O. S. Wolfbeis, *Microchim. Acta* **2008**, *162*, 1.
- [52] E. Shoji, M. Freund, *J. Am. Chem. Soc.* **2002**, *124*, 12486.
- [53] B. Deore, M. S. Freund, *Analyst* **2003**, *128*, 803.